Cancer Nanotechnology

RESEARCH Open Access

Carbon nanoparticles induce DNA repair and PARP inhibitor resistance associated with nanozyme activity in cancer cells

Haiyan Fan[1†], Qinglei Sun[2†], Kanat Dukenbayev[3†], Enrico Benassi[4†], Limara Manarbek[5], Ayan A. Nurkesh[5], Medina Khamijan[5], Chenglin Mu[6], Guoliang Li[7], Madina Razbekova[5], Zhenbang Chen[7], Amr Amin[8] and Yingqiu Xie[5*]

†Haiyan Fan and Qinglei Sun are co-first authors and contributed equally to this work

†Kanat Dukenbayev and Enrico Benassi contributed equally to this work

*Correspondence: yingqiu.xie@nu.edu.kz

[5] Department of Biology, School of Sciences and Humanities, Nazarbayev University, Astana 010000, Kazakhstan
Full list of author information is available at the end of the article

Abstract

Background: Quantum nanodots especially carbon nanoparticles (CNPs) have been widely studied in biomedicine in imaging, and drug delivery, but anti-cancer mechanisms remain elusive.

Methods: Here, we investigated a type of cell death induced by food (beet, soybean) derived CNPs in cancer cells and tested whether CNPs induced DNA damage and resistant to anti-cancer agent PARP inhibitor (PARPi) could be overcome by quantum calculations, TEM, AFM, FT-IR, soft agar assay, and cytotoxicity assay.

Results: At high doses, CNPs derived from beet lead to a pop-like apoptosis (Carbopoptosis) in cancer cells. Quantum mechanical calculations confirmed CNPs binding with phosphate groups as well as DNA bases. At low doses, CNPs develop PARPi drug resistance through interactions between CNPs and PARPi. A synergistic drug effect was achieved with the combination of phosphatase inhibitor (PPi), PARPi, and CNPs. This is corroborated by the fact that sulfur modulated CNPs which exhibit super high phosphatase nanozyme activity abrogated the CNPs induced colony formation in anchorage-independent cancer cell growth.

Conclusion: Thus, our data suggest the CNPs intrinsic nanozyme activity of phosphatase may crosstalk with drug resistance, which can be reversed upon modulations.

Keywords: Carbon nanoparticles, PARP inhibitor, Drug resistance, Carbopoptosis

Background

Carbon nanoparticles (CNPs) especially carbon nanodots (CDs) represent nanoscale carbon particles or aggregates containing mainly carbon, oxygen and hydrogen, and sometimes also nitrogen, sulfur and phosphorus, in the form of organic functional groups distributed on the surface of these particles or aggregates. Based on such a concept, natural metabolite in diet, the burning product of plant wastes can all be classified as CNPs (Wang et al. 2020). With virtues of low cost, high biocompatibility, strong photoluminescence, solubility, and flexibility for surface functionalization, CNPs have been

widely applied in the development of nanomedicine (Wang et al. 2020; Chen et al. 2021). One of the main advantages of nanoscale CDs in drug delivery and imaging, is their non-toxicity or extremely low toxicity (Xu et al. 2015; Miao et al. 2015; Li et al. 2014; Hsu et al. 2013; Xie et al. 2017, 2019; Lou et al. 2022; Zheng et al. 2022).

In anti-cancer therapy, cell death is usually through a toxicity-driven mechanism among classified cell deaths such as apoptosis, necrosis, autophagy, pyroptosis, and oncosis (D'Arcy 2019). As far as nanoparticle-induced cell death is concerned, there are mitochondrial stress, autophagy, membrane abolish mediated cell death, Golgi damage induced adhesion loss, and neutrophil apoptosis (Kirwale et al. 2019; Xiao et al. 2019; Zhang et al. 2019; Gong et al. 2019; Ma et al. 2019). Nevertheless, the mechanisms underlying the inhibition of the cancer cell growth or induced cell death by CNPs have been paid very little attention, particularly at omics levels. Coincident with a recent report on CNPs induced cell death directly mediated by p53 (Li et al. 2014). We previously reported that CDs may deregulate ARF-YAP signaling, co-target mTOR, MET, and Pim-1 kinases through combinatorial inhibition of cancer cell growth (Xie et al. 2017, 2019; Nurkesh et al. 2019).

Poly (ADP-ribose) polymerase (PARP) protein family plays essential roles in the default single-strand DNA (ssDNA) repair to maintain genomic stability (Lord and Ashworth 2017). However, in the cancer therapy targeting the cancer cell DNA, such ssDNA, repairing could become chemoresistance. Therefore, PARP inhibitor (PARPi) emerged as a promising agent used together with anti-cancer medicines (Lord and Ashworth 2017). PARPi has been introduced in the clinical trials to treat ovarian and prostate cancers (Lord and Ashworth 2017; Kim et al. 2017; Clarke et al. 2018). In particular, concurrent targeting DNA damage using PARPi and anti-cancer agents intervening the signaling pathways have been utilized to achieve synergistic cytotoxicity in cancer cells, namely synthetic lethality, which has been widely applied to much other cancer therapies (Coleman et al. 2015; O'Neil et al. 2017).

Given that CNPs potentially cause DNA damage (Xie et al. 2019; Singh et al. 2018), the present work explores the potential CNPs induced cell death signaling and combinatorial with PARP inhibitors to develop a novel conceptual link of carbon effect on cancer therapy.

Materials and methods

Synthesis of carbon nanoparticles, FT-IR, XPS, fluorescence spectra and quantum chemical calculations

In a 100-mL autoclave reactor, 3 g of dried beet or soybean powder, 24 mL ethylenediamine and 36 mL of deionized water were mixed well, followed by a hydrothermal reaction at 200 °C for 5 h. The liquid product was then collected through filtration and underwent centrifuge and dialysis for 48 h (1000 Da). The final product was obtained by placing the liquid product in a vacuum oven at 60 °C overnight. S-doped CNPs were produced in the exact same process except that 2 g of sulfur powder was added in the system for the hydrothermal reaction. The stock solution of CNPs was prepared by weighting a certain amount of dried product (sticky) and adding deionized water to the desired volume. The present work involves 10 batches of CNPs and 3 batches of S-doped CNPs. XPS spectra were collected using a *X*-ray photoelectron spectrometer (Nexsa,

Thermo Scientific). We found that the morphology, FT-IR, UV–Visible and fluorescence spectra along with the biological properties have not shown any batch dependence. IR spectra were recorded using a Thermoscientific Nicolet IS5 FT–IR spectrometer in the range from 500 to 4000 cm^{-1} at the resolution of 2 cm^{-1} and on the diamond ATR. Fluorescence emission was scanned on a spectrometer (Agilent Cary Eclipse) in the range from 400 to 800 nm. The computational details were described in the previous work (Xie et al. 2019).

Differentially expressed protein shotgun sequencing and analysis

PC3 cells were treated by soybean and beet CNPs at 0.1 mg/mL for 2 h, and then total proteins were extracted and subjected to SDS-PAGE gel separation with staining and differential expressed proteins were isolated from the gel at a molecular weight of 100 kDa and 70 kDa followed by shotgun sequencing of proteins. Using the NpSpCk quantitative method, the shotgun identification results are quantified (Cox and Mann 2008; Wiśniewski et al. 2009; Sandberg et al. 2012; Callister et al. 2006). For the quantitative results, the protein expression difference analysis between the two groups of samples was performed. FC, fold change was calculated. The *p*-value obtained from the *T*-test is used to draw a volcano graph, which is used to show the significant difference between the two sets of sample data (only in one group, but not in the other group). The abscissa is the difference multiple (logarithmic transformation based on 2), and the ordinate is the significant *p*-value of the difference (logarithmic transformation based on 10).

The interaction maps for beet CNPs induced differential levels of proteins were constructed using the Cytoscape software (Shannon et al. 2003) based on the protein list obtained from the sequencing. The circular layout was set to obtain a meaningful map where the colors were arranged using the STRING tool (Szklarczyk et al. 2019). Enrichment was performed using the StringApp plugin (Doncheva et al. 2019) and Kyoto Encyclopedia of Genes and Genomes (Kegg) pathway (Kanehisa et al. 2019), where the colors were set manually that correspond to the pathways outlined. The distinct pathways were labeled in contrast to common. For the GO and pathway analysis, the DAVID tool was applied (Huang et al. 2009). The induced protein differentially expressed by two types of CNPs were analyzed by Venny 2.1 sorting out common intersections networks and reactome, transcription network analysis were performed by online tools (https://bioinfogp.cnb.csic.es/tools/venny/index.html; http://www.licpathway.net/KnockTF/analysis/analysis_submit_gene.php) (Oliveros 2007–2015; Fabregat et al. 2017; Li and lab KnockTF online database).

High-resolution atomic force microscopy (HR-AFM), transmission electron microscope (TEM), confocal microscopy and live phase-contrast microscopy

Cells were plated on a coverslip pretreated with polylysine on the surface for HR-AFM measurements. Cells were subjected to fixation after attached by overnight. Then cells were quickly dried before performing HR-AFM investigation. For DNA binding assay, DNA and CNPs were incubated in Eppendorf tube for 30 min then directly were put on a coverslip for air dry with washing by PBS before carrying out HR-AFM. DNA and CNPs mixtures were also subjected to agarose gel electrophoresis.

For TEM, aqueous solution of CNPs was loaded on PELCO grids for investigation. For confocal assay, cells were plated in coverslip and treated by CNPs followed by fixation and staining by the protocol of Cell Signaling Inc. The antibodies used are Phosphor-FAK (Tyr397) (Invitrogen), AQP5 (D-7)(Santa Cruz Biotechnology), MMP7(R&D Systems), Gasdermin (Santa Cruz Biotechnology) and DAPI for staining the nucleus (Invitrogen). Coverslips were mounted using Fluoromount and investigated by Carl Zeiss LSM780 confocal microscope. The objective lens used is 40X or 63X Oil. For live phase-contrast microscopy, cells were examined by EVOS Floid Cell imaging station.

Soft agar, cell cycle, cell death, and cell viability assays

Cells were grown in soft agar according to methods described previously (LeCory et al. 2017). For cell cycle, PC3 cells were treated with 1xPBS vehicle or CNPs (0.1 mg/mL) for 2 h. The cell cycle analysis was performed using a Muse® Cell Cycle Kit (MCH100106, Merck Millipore). For cell death assay, PC3 cells were treated with CNPs or vehicles (PBS) as described previously (Nurkesh et al. 2019). Cell staining was performed under instructions from Muse® Caspase-3/7 Assay Kit (MCH100108, Merck Millipore), Muse® Annexin V & Dead Cell Kit (MCH100105, Merck Millipore), and samples were run by Muse cell analyzer (Merck Millipore). Cell viability assay was performed as described previously (Xie et al. 2019).

Results

CNPs induce a novel rescueable cell toxicity—carbopoptosis

Morphological and chemical characterization of CNPs

The morphology of CNPs derived from beet were characterized using TEM (Fig. 1a), and AFM (Fig. 1b). While TEM image indicate a circle shape with an average diameter of ~ 140 nm, the AFM image exhibits a cylindrical shapes with an average diameter of 123–135 nm and average thickness ~ 40 nm. Overall, the CNPs derived from beet show a morphology of right circle cylinder. CNPs derived from soybeans indicate very similar morphology. The XPS spectra (Fig. 1c) reveal the hybridization status of the elements such as C, N, O located on the surface of the CNPs (Fig. 1d). The survey spectrum shows C1s, N1s and O1s are involved in the CNPs (Fig. 1e). Three main peaks are deconvolved in the high-resolution scan of C1s: peak at 284.6 eV represents the C in C–C form, 285.6 eV, C in C–N bond and 287.5 eV stands for the C in C=O functional group. There are two peaks at ~ 293 eV and 295 eV in C1s spectrum, showing nonnegligible intensity. These peaks were identified by Nishii *et al*. as the K 2p, which could be caused by impurities containing K (Fujioka et al. 2017). N is in a form of C=N and N–H evidenced by the high-resolution peaks at 398.8 eV and 399.8 eV, respectively (Fig. 1f). High-resolution peaks for O 1s at 530.7 eV and 532.1 eV represent O in C=O and C–O bonds, respectively.

Consistent with XPS, the FT-IR spectrum of Beet CNPs (Fig. 2a) indicates a typical amide functional group distributed on the surface, which is featured with the absorption band at 1648 cm^{-1} representing C=O stretching vibration, 1558 cm^{-1} corresponding to N–H bending vibration, 1323 cm^{-1}, C–N stretching vibration, 3258 cm^{-1} and 3315 cm^{-1} representing N–H stretching vibration. The aqueous solution of CNPs derived from both beet and soybean emits light blue/green fluorescence under irradiation of a UV-lamp

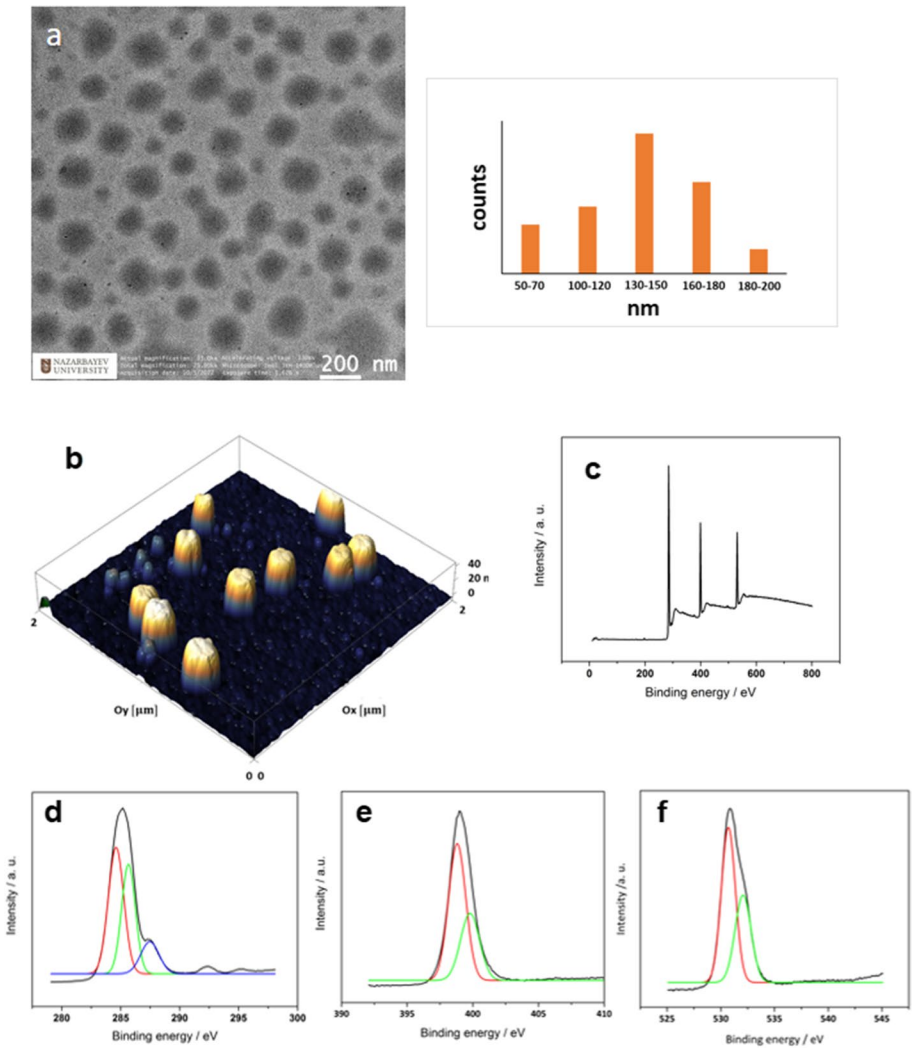

Fig. 1 Characterization of carbon nanoparticles (CNPs) derived from beet. TEM (**a**), AFM (**b**) images and XPS spectra of CNPs from beet: survey scan (**c**); high-resolution scans for C1s (**d**), N1s (**e**) and O1s (**f**)

at 365 nm (Fig. 2b). The systematic measurements show the fluorescence is excitation wavelength dependent. Such excitation wavelength dependence of fluorescence is rather common among CNPs and carbon quantum dots, which is rationalized by two distinct deactivating paths upon excitation (LeCory et al. 2017).

Upon treatment at the dose of 0.25 mg/mL, both types of CNPs induced osmosis resembling cell burst (Additional file 5: Fig S1a). Through the snapshot videos, the nature of the cell death was revealed as non-canonical cell death. In specific, the prostate cancer PC3 cells initially transited into a spherical shape, followed with detachment, and finally burst within 30 min (Additional file 5: Fig. S1a, Additional file 1: Video S1, Additional file 2: Video S2, Additional file 3: Video S3 and Additional file 4: Video S4). Adding the hypotonic osmosis induced by 2.5M glucose to the solution of CNPs, cell burst was found to be accelerated. Even after the treatment with 10M glucose, the shriveled cells were swollen again upon the addition of the solution of CNPs

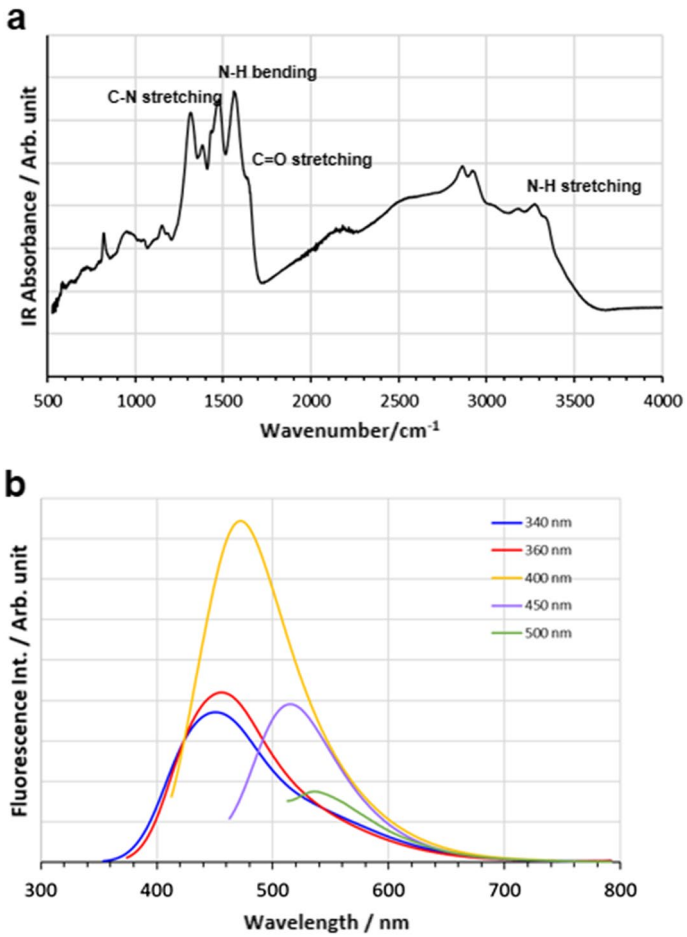

Fig. 2 FT-IR spectrum of beet CNPs (**a**) and fluorescence spectra at different excitation wavelengths (**b**)

(Additional file 5: Fig. S1b, Additional file 1: Video S1, Additional file 2: Video S2, Additional file 3: Video S3, and Additional file 4: Video S4). Moreover, CNPs induced detachment was investigated by re-plating. After 5 or 24 h, control cells were almost spread, whereas CNPs treated cells mostly exhibited detachment morphology (Additional file 5: Fig. S1a). Meanwhile, the extracellular matrix (ECM) molecules, such as fibronectin and Matrigel, were able to prevent the detachment (Shi 1995) and eventually reverse the CNPs induced cell death (Additional file 5: Fig. S1b). CNPs might trigger a non-specific phosphatase replacing the extracellular phosphatase, which is essential for the ECM cellular functioning, leading to the detachment and further cell death. Our data suggest the CNPs mediated detachment is associated with cell death, which is similar to anoikis (Shi 1995; Vivo et al. 2017). Such observation finds support from our previous work with tea-derived CDs, wherein, CDs stimulated $p14^{ARF}$ expression (Xie et al. 2017), while $p14^{ARF}$ is closely related to the anoikis including changes in FAK (Vivo et al. 2017). We further collected and kept culturing the detached spherical cells using a fresh medium. Surprisingly, the cells continually grew into a larger size than that of the vehicles (Additional file 5: Fig. S1b, c). The HR-AFM images indicated the cell morphology changed into a spherical shape induced

by CNPs and further revealed the caused cell death likely is through the loss of lamellipodia and displayed how fibronectin may counteract such effect (Fig. 3a).

Using confocal microscopy, we tested the cell marker of pyroptosis, Gasdermin (Fang et al. 2020), and no significant change was observed upon the addition of CNPs, which renders the enhanced level of ECM-related marker MMP7 (Fig. 3b). The fact that CNPs stimulated the translocation of osmosis-related water channel protein AQP5 to the membrane suggests that water transportation is responsible for the cell swelling and burst (Fig. 3b). Labeled with phosphor-FAK, the confocal images in Fig. 3f also indicated that CNPs significantly reduced the focal adhesion in PC3 cells. Finally, cell death caused by both types of CNPs was related to Annexin V, caspase 3/7, and induce cell cycle arrest at G0/G1, or G2/M in prostate cancer PC3, as well as the normal rat kidney (NRK) cells (Additional file 5: Fig. S1e, f). Compared to the beet CNPs, soybean CNPs showed much less Caspase 3/7 related cell death in normal NRK cells. While both CNPs exerted a similar effect on cell osmosis-associated death, they demonstrated a difference in Caspase 3/7, suggesting the potential of a novel type of cell death linked to CNPs.

In summary, low-dose CNPs induced cell death is transient, acute, and rescueable through the regulation of osmosis-related phenotype. Based on such a unique type of cell death induced by CNPs, we then initiated a definition of carbopoptosis representing the carbon particles induced pop-like apoptosis.

Signaling pathways analysis of CNPs induced carbopoptosis

To explore the signaling pathways of CNPs induced cell death, we applied a protein shotgun analysis of expressed proteins with significant upregulation on SDS-PAGE gel separation upon treatment in PC3 cells and performed GO, protein network analysis

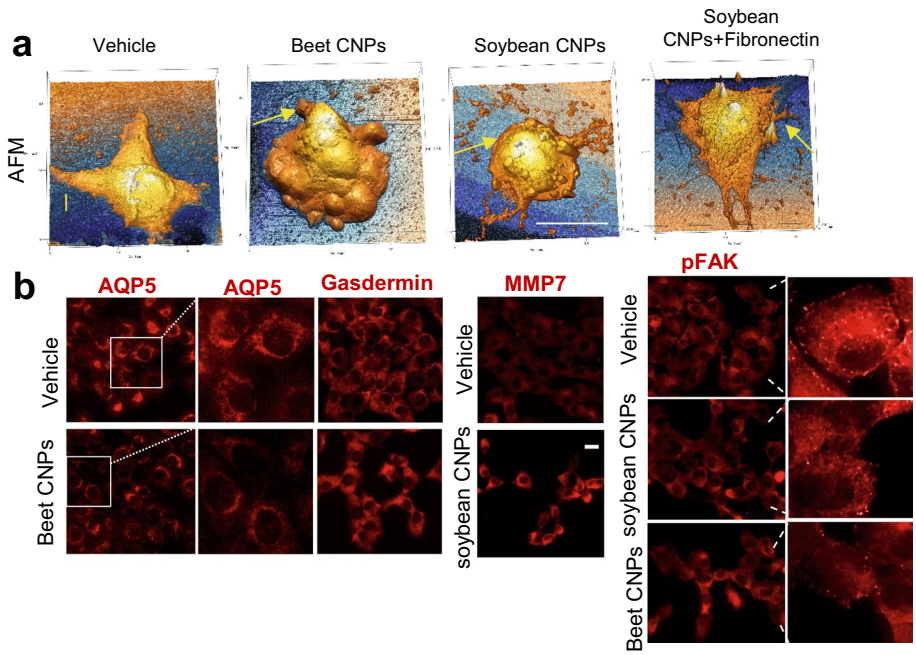

Fig. 3 CNPs induce a novel cell death of carbopoptosis. (**a**) High-resolution (HR)-AFM images of PC3 cells undergoing detachment and inhibition by fibronectin. Scale bar, 5 μm (**b**) Confocal microscopy of PC3 cells treated by CNPs at 0.1 mg/mL for 2 h. Objectives 40X. Scale bar, 20 μm

(Fig. 4a). In bioinformatics, GO is used in the analysis of gene lists for an explanation of bio-effect. The biological analysis of GO further revealed the cell cycle regulation, DNA damage, and apoptosis (Fig. 4b). The results indicated that soybean and beet CNPs induced similar upregulated pathways with minor specificity on both pathways with co-targets of 58% including cell death-related gene clusters (Fig. 5a). Many protein–protein interaction network nodes and KEGG pathways relate to phosphorylation-dephosphorylation/mTOR kinases, cell death, DNA binding, and DNA damage/DNA repair (Fig. 5b). More importantly, GO analysis also demonstrated that the DNA repair protein pathways were affected by both soybean and beet CNPs which are upregulated compared to the control by reactome analysis (Fig. 5a).

The *p*-value obtained from the *T*-test is used to draw a volcano graph, which shows the non-significant difference between the two types of CNPs treated PC3 cells (Fig. 5c). Our data suggest the similar mechanisms of both types of CNPs regarding the effect on cell signaling, however, some pathways may be selective for one kind CNPs over the other kind due to the subtle difference in the chemical compositions or morphology.

Further tests were arranged to identify whether the CNPs may induce DNA damage response in cells. As indicated in Fig. 5d, elevated DNA damage marker γH2AX was reproducibly detected after the treatment of beet CNPs (Additional file 5: Fig. S2). DNA damage was found occurring in the nucleolus region right across to BRCA1 (Fig. 5e). Thus, the DNA damage repair might be related to PARP, as BRCA1 is usually complementary to PARP failure. Tail DNA counting also suggests the damage repair is related to the soybean CNPs-induced cell death (Xie et al. 2019).

CNPs bind to DNA indicated in quantum chemical calculations and induce DNA damage/mutation

The direct interaction between CNPs and DNA was explored in vitro. As indicated in Fig. 5d and Additional file 5: Fig. S2, elevated DNA damage/repair marker γH2AX was detected after the treatment of both soybean CNPs (Xie et al. 2019) and beet CNPs and colocalization can be found (Fig. 5e). It was observed that the particles of both CNPs carry positive charges as revealed in the electrophoresis tests displayed in Fig. 6a. CNPs

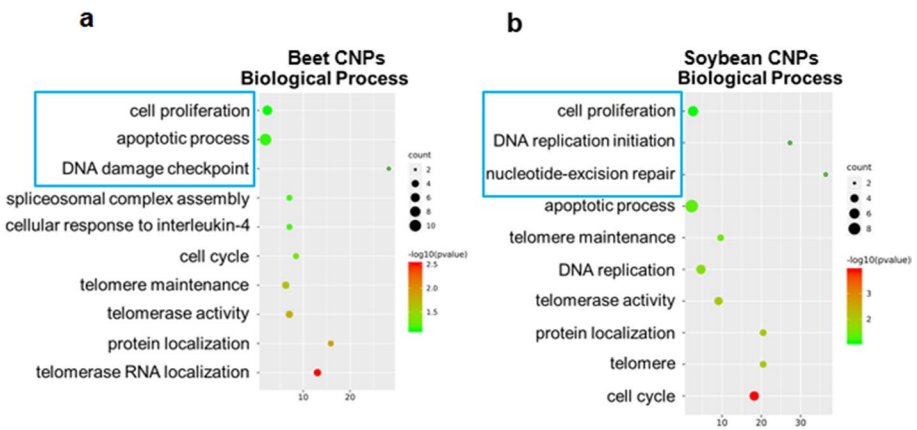

Fig. 4 CNPs induced network and clusters of cell signaling by protein shotgun analysis upon CNPs treatment of PC3 cells. **a**, **b** GO enrichment analysis and details in biological process of soybean CNP and beet CNP

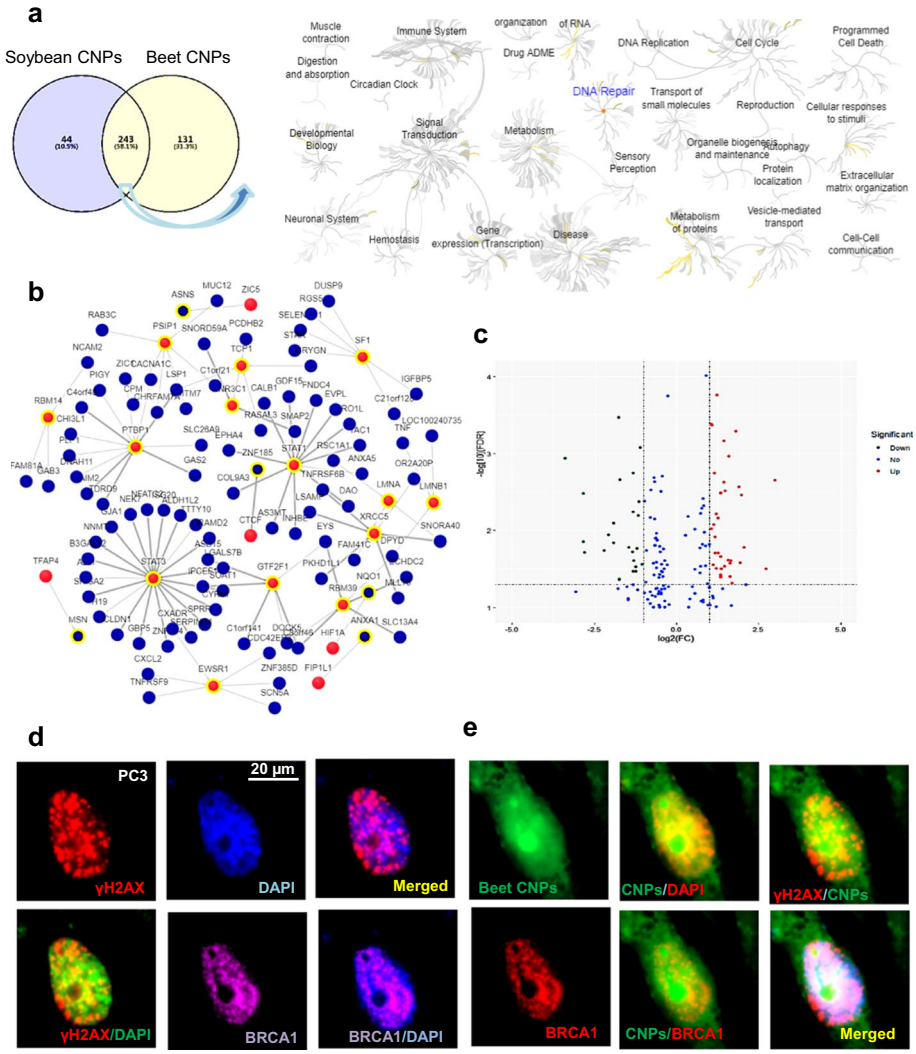

Fig. 5 CNPs induced common pathways analysis. **a** Venn diagram of the soybean and beet CNPs target proteins of intersections. Reactome analysis showing DNA repair is highly enriched in intersections. **b** Protein–protein interaction network topology with nodes. **c** Volcano plots of the proteins quantified during the shotgun sequencing data. The green dots are significantly down-regulated proteins; the red dots are significantly upregulated proteins (fold change is more significant than 1.2 times and *p*-value < 0.05), and the blue dots are proteins with no significant changes. **d**-**e** Confocal images of PC3 cells DNA repair induced by beet-derived CNPs. Scale bar, 20 μm. Different counter acting colors were used from the original confocal color for indicating the merged effect. For example, CNPs (green) and BRCA1(red) colors are merged as yellow, indicating less co-localizations

were found binding with single-stranded DNA (ssDNA) to form a complex carrying overall negative charges. On the other hand, the binding of CNPs with double-stranded DNA (dsDNA) slowed down the migration of ds-DNA toward the positive electrode, and the bands were slightly more spread out than DNA alone, indicating the binding with CNPs partially neutralizes some negative charge on dsDNA without causing the fragmentation of DNA (Fig. 6a). In a separate experiment shown in Fig. 6b, negatively charged glutamine (GLU) and SDS were added to CNPs, a strong disruption of charge was observed between soybean-CNPs and SDS, wherein the fluorescence of CNPs was

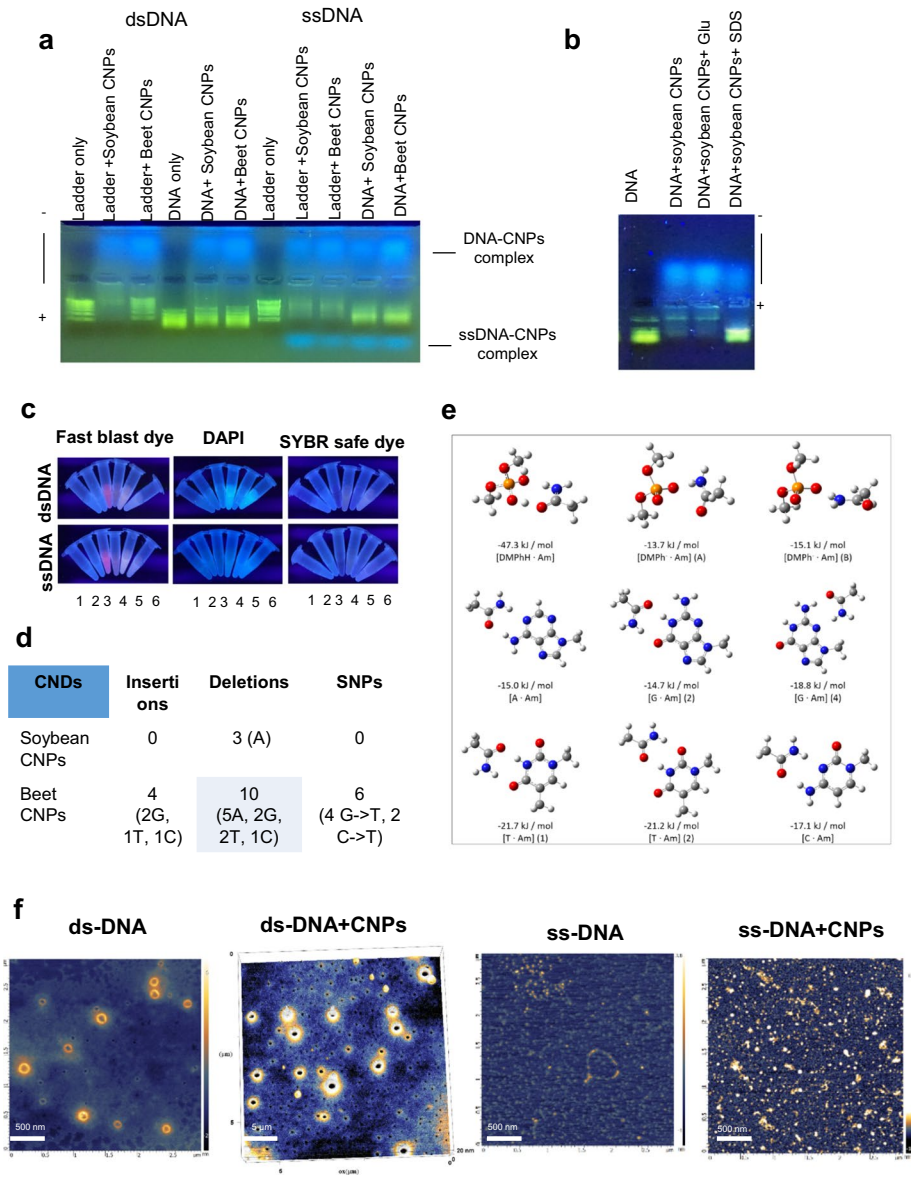

CNDs	Insertions	Deletions	SNPs
Soybean CNPs	0	3 (A)	0
Beet CNPs	4 (2G, 1T, 1C)	10 (5A, 2G, 2T, 1C)	6 (4 G->T, 2 C->T)

Fig. 6 Carbon nanoparticles bind DNA, induce DNA mutation, and cause DNA damage repair response through PARP. **a** CNPs bind double-strand (ds) or single-strand (ss) DNA detected by DNA agarose gel electrophoresis. **b** Negative charges by Glu or SDS interfere with the binding. **c** CNPs compete with dyes to bind DNA. 1. soybean CNPs; 2. soybean CNPs and DNA; 3. dye; 4. dye and DNA; 5. soybean CNPs and dye; 6. soybean CNPs, dye, and DNA. **d** DNA mutations induced by CNPs-DNA interactions in a plasmid sequencing. **e** Optimised geometries of HB complexes modeling DNA and CNPs interaction modes. Legend of colors: white (H), grey (C), blue (N), red (O), and orange (P). **f** HR-AFM images of CNPs binding to DNA circular forms of plasmid DNA. Scale bar, 5 μm or 500 nm as indicated

significantly quenched, and DNA was mostly left alone. To identify the nature of the binding between DNA and CNPs, a competitive analysis was performed with DNA dyes, wherein Fast blast dye and SYBR showed the better binding competition with CNPs binding to DNA suggesting the CNPs bind to the similar position of phosphate groups on DNA (Fig. 6c) (http://www.bio-rad.com/webroot/web/pdf/lse/literature/Bulletin_4110153A.pdf).

Our previous work indicated soybean/beet-derived CDs interact with phosphate group leading to the dephosphorylation of tyrosine phosphate (Xie et al. 2019), and our another work revealed S-doped CNPs accomplish the phosphatase through its SH group (unpublished work).

The FT-IR spectrum of beet-derived CNPs is almost identical to that of soybean-derived CNPs, and both indicated vibrational bands representing C=O stretching, N–H bending, C–N stretching and N–H stretching, which is a typical amide characteristic. Therefore, it is possible to study the potential hydrogen bonding interaction not only between CNPs and backbone phosphate groups on DNA, but also between CNPs and bases of DNA.

Quantum mechanical calculations at the DFT level were performed to model the interaction between CNPs and DNA, in particular, to estimate the energetics of the interaction, and describe its nature. Both CNPs and DNA are macro-molecules, which are too large to be investigated from a quantum mechanical (atomistic) level. Simpler models based on the scaffold containing the key functional groups were used in the input file (Fig. 7). Concerning CNPs, we shall adopt acetamide. Concerning DNA, from a chemical point of view we expect that the possible interaction may occur between acetamide and either the backbone phosphate group or the nitrogenous bases (NBs). We, therefore, built models of these two moieties. Four bases NBs (A, G, T, and C) were considered in the methylated form. About the phosphate group, we believe that dimethyl phosphate (DMPh) may represent a computationally reasonable yet chemically meaningful model of the phosphate group on DNA backbone. Depending on the pH of the surrounding environment, DMPh may be protonated, (CH3)2-OPO3H, or deprotonated,

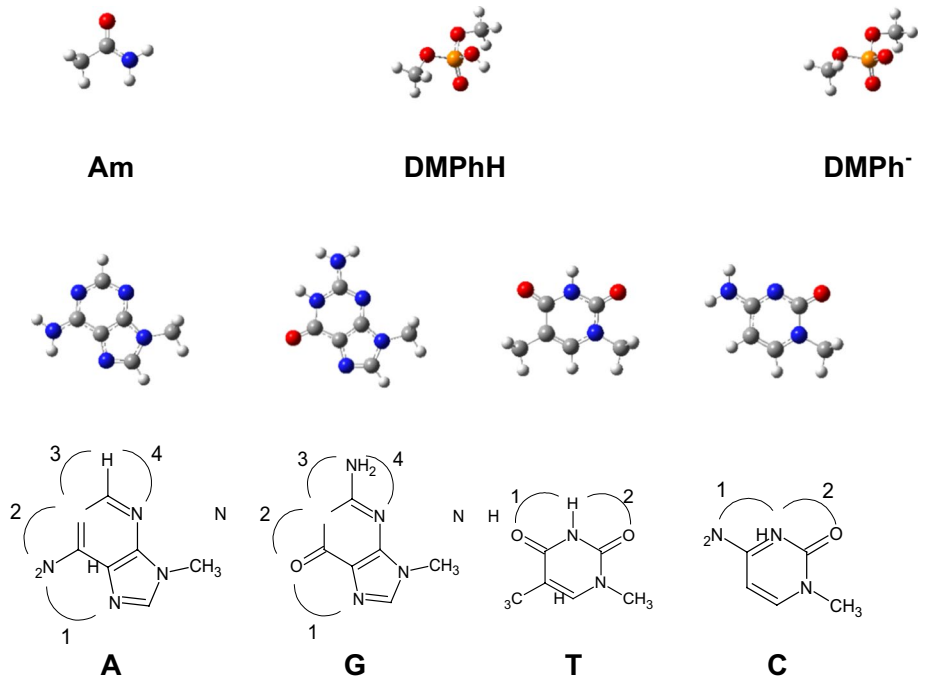

Fig. 7 Molecular models and attack positions on NBs. Legend of colors: white (H), grey (C), blue (N), red (O), and orange (P)

(CH3)2-OPO3- (namely DMPhH and $DMPh^-$, respectively). In our investigation, we computed both of them. Possible interactions between acetamide (representative of CNPs) and dimethyl phosphate/NBs (representative of DNA) are intended as hydrogen bonds. Each monomer contains two or more centers (groups) that are H-bonding active; in particular, these centers may act as H-acceptor (A) and H-donor (D). Concerning NBs, there are two to four possible attack positions for A and T and two for C and G (Fig. 7). When dimers are built, different possible configurations and rotamers are considered and investigated.

Figure 6e shows the geometries of the most stable dimers; the values of dimer formation enthalpy are also depicted. The values of formation enthalpy computed for all the dimers are summarized (Table 1).

The strongest interaction occurs between the amide group of CNPs and the phosphate group of the DNA backbone (DMPhH); such an interaction is stabilized through a double H-bonding, where quantum chemical calculations show that one of the two implies a proton sharing between DMPhH (H-donor) and the carbonyl oxygen of Am (H-acceptor). The interaction between the phosphate group and the CNPs is still quite strong even when the former is deprotonated ($DMPh^-$). In this case, a single H-bond is shown. This indicates that the CNPs can attack the DNA phosphate backbone in a quite wide pH range.

In addition to DMPhH and $DMPh^-$, Am may form stable intermolecular interactions with NBs, in any attack position marked in (Fig. 7), via one or two H-bonds. In particular, G and T show two possible attack positions for double H-bonding. Overall, the H-bonding between Am and T at the binding position 1 and 2 is the strongest among all the possible dimers formed by Am and NBs, followed by the H-bond with G at the binding position 4.

Table 1 The interaction energies (kJ/mol) for all the possible dimers formed between acetamide and phosphate group and those between acetamide and nitrogen bases

DNA	CNPs	Position	Rotamer	Δ*H*/(kJ/mol)
DMPhH	Am			− 47.3
$DMPh^-$	Am		A	− 13.7
			B	− 15.1
A	Am	1		− 14.6
		2		− 15.0
		3		− 6.1
		4		− 7.6
C	Am	1		− 17.1
		2	A	− 9.4
		2	A	− 13.0
		2	B	− 10.2
G	Am	1	A	− 5.7
		1	B	− 7.2
		2		− 14.7
		3		− 4.3
		4		− 18.8
T	Am	1		− 21.7
		2		− 21.1

Summarizing, quantum chemical calculations indicate that the strong intermolecular interaction driven by proton sharing from the backbone phosphate group on DNA to CNPs is essential for the activation/deactivation mechanism. Consider the working pH, as well as the amount of ethylenediamine was used in the synthesis of CNPs, the protonated amine group was put into the consideration that potentially take responsibility of positive charge of CNPs (Kokorina et al. 2019; Sai et al. 2017; Li et al. 2018). These protonated to potentially interact with DNA. Quantum mechanical calculations indicated a large positive ΔG value for such interaction meaning the protonated ethylenediamine unlikely interacts with NBs. On the other hand, the results of both FT-IR and XPS showed amide rather than amine (protonated or neutral) is dominated functional group distributed on the surface of CNPs. On the other hand, the binding between CNPs and NBs is quite significant based on the energy, which is competitive with that occurring between the two helixes ($\Delta H(A{\cdot}T) = -$ 23.3 kJ/mol; $\Delta H(C{\cdot}G) = -$ 36.7 kJ/mol), it is expected that CNPs may lead to the fragmentation of DNA (Table 1).

Sanger sequencing of partial plasmid DNA suggests a broad range of single nucleotide deletion and insertion (Fig. 6d). Further evidence for the strong binding between DNA and CNPs was provided by HR-AFM imaging and depicted in Fig. 6f, the added CNPs were accumulated on the outline of the coil-shaped ds-DNA suggesting the strong interaction between CNPs and the backbone phosphate on DNA. As for the single-strand DNA, the addition of CNPs dramatically enhances the fragmentation, an indication of the strong binding between CNPs and bases on the chain of ss-DNA.

CNPs induced carbopoptosis is related to the DNA repair pathway and low-dose CNPs can mediate drug resistance to PARP inhibitor

Soybean derived CNPs can inhibit tumor cell growth when applied in alone. However, at low dose, the combination of CNPs and PARP inhibitor (PARPi), olaparib, promotes tumor growth compared to PARPi alone, suggesting CNPs may induce drug resistance toward olaparib in two different cell lines, cervical cancer HeLa cells (Fig. 8a) and prostate cancer DU145 cells (Fig. 8b). Though the low-dose CNPs induce drug resistance to PARPi, high-dose CNPs exhibited the synthetic lethality with PARPi (Fig. 8b). The results imply the dose plays an essential role in the cell fate as for being resistant or sensitization. Herein, we propose a novel CNPs induced reversible, i.e., repairable "cell death" and its mechanism by PARP. On the other hand, caution should be taken when applying low-dose CNPs as a drug delivery carrier for PARPi, lest drug resistance may occur.

CNPs mediated drug resistance can be overcome by inhibiting co-phosphatase activity from inducing "synthetic lethal"

Given that CNPs act in competition with PARPi to develop drug resistance through intrinsic phosphatase-like activity, which deregulates many pathways including DNA damage, kinase, and dephosphorylation, we then proposed to apply a protein phosphatase inhibitor (PPi) to suppress phosphatase and subsequently overcome drug resistance. PPi was then used to treat cancer cells along with the combination of the CNPs with PARPi, and the cytotoxicity assay indicated that the PPi enhanced sensitization of CNPs and also reversed the low doses of CNPs-mediated drug resistance toward PARPi

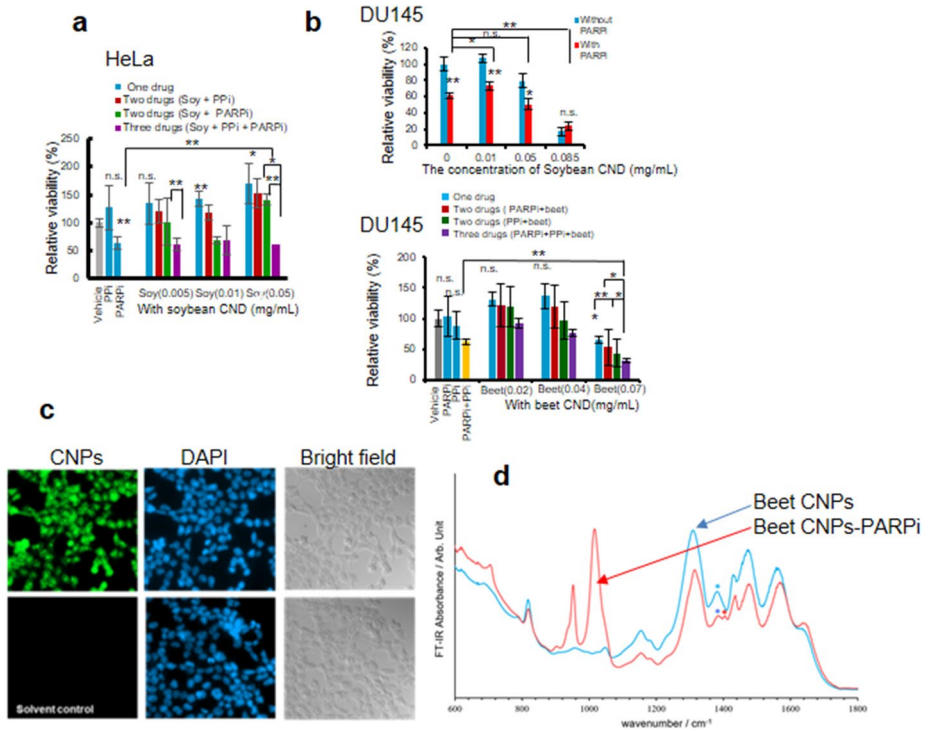

Fig. 8 CNPs mediated cell death is reversed by PARP inhibition and can be overcome by phosphatase inhibition to induce synthetic lethality. **a** CNPs resistant to PARP inhibition by olaparib at low dose and combined treatment by PPi. **b** CNPs resistant to PARP inhibition by olaparib at low dose but not in high dose. **c** Beet CNPs distribution in HELA cells. **d** The comparison of the FT-IR spectra for beet CNPs and the combination with PARPi (Olaparib)

(Fig. 8b). The CNPs intrinsic fluorescence which was used to monitor the CNPs cellular localization, showed nucleus-predominant distribution in HeLa cells (Fig. 8c).

The "synergetic lethality" achieved through the combination of high-dose CNPs and PARPi is likely due to an intermolecular interaction between CNPs and PARPi. The comparison of FT-IR spectra between CNPs and the mixture of CNPs and PARPi indicates while C=O stretching (1633 cm^{-1}) and N–H bending (1557 cm^{-1}) absorption in amide groups remain nearly the same upon mixing with PARPi (Fig. 8d), the absorption band at 1380 cm^{-1} representing C–N stretching in Amide I split into two peaks at 1388 cm^{-1} and 1403 cm^{-1}, respectively. Meanwhile, one of the N–H stretching bands, originally located at 3348 cm^{-1} shifts to 3356 cm^{-1} upon mixing with PARPi. Both band splitting reflected in C–N stretching and the band shift in N–H stretching confirm the strong interaction between CNPs and PARPi likely through intermolecular hydrogen bond, wherein -NH in amide group acts as the hydrogen bonding donor.

The present results suggest the CNPs might be applied in cancer therapy as the future "green anti-cancer reagents". It is hypothesized phosphatase-like activity mediates drug resistance toward PARPi, and the PPi may help to overcome such resistance. The CNPs mediated drug resistance against PARPi was likely due to their strong affiliation with the protein phosphate and DNA backbone phosphate. The present work provided profound insight into the drug resistance development, as well as the caution in the usage

of carbon nanoparticles-based delivery of DNA damage-themed drugs such as PARPi in cancer therapy.

Enhanced phosphatase nanozyme activity of CNPs by sulfur doping disrupts the CNPs efficiency on anti-cancer cell growth

To pin down the role of phosphatase activity in CNPs anti-cancer function, sulfur-doped beet CNPs (Beet SS) were synthesized as mimics of protein phosphatase. A stronger phosphatase activity of Beet SS than that of beet CNPs was identified using a phosphatase substrate (Additional file 5: Fig. S3a). Beet SS CNPs decreased the efficiency of anti-colony formation compared to beet CNPs, i.e., the enhanced anchorage-independent growth with less cell death simulating 3-D like properties than the undoped CNPs (Additional file 5: Fig. S3b). Our data suggest the phosphatase activity of CNPs at least in part, associates with the CNPs-mediated anti-cancer activity.

Discussion

We herein report that CNPs may mediate a repairable "cell death" to induce phosphatase-related drug resistance through their binding to the phosphate groups. Caution should be paid when CNPs-based drug delivery is carried out at a low dose. Nevertheless, such drug resistance developed by CNPs may be overcome upon the addition of PPi, and consequently, the strategy by generating a cocktail treatment by the combination of low doses of CNPs, PPi, and PARPi finally renders a synergetic "lethality".

In our recently published work, CDs derived from date pits were found to mediate DNA damage related to BER or NER pathways which are consistent with the investigation of other nanoparticles (Nurkesh et al. 2019; Kad et al. 2010). While ligation steps play essential roles in DNA repair as the last step of both BER and NER, CNPs develop a potential inhibition against DNA ligation via dephosphorylation. The CNPs induced dephosphorylation is rooted on the strong interaction identified between CNPs and the phosphate on the DNA backbone evidenced both in experimental and quantum mechanical perspectives. There are no key links to differentiate CNPs derived from different resources, but they have common signaling in DNA repair, which provided reasonable mechanisms of the CNPs induced DNA repair and PARP inhibitor resistance in cancer cells by identified gene regulation profiling from proteomic experimental data. The advantages did not show the CNPs from one to another.

In our previous study, soybean-derived CNPs were identified to resemble the protein tyrosine phosphatase (PTP) (Xie et al. 2019), wherein, the interaction energy between soybean CNPs through protonated amide group and protein tyrosine phosphate is − 62.7 kJ/mol according to quantum mechanical calculations, which is more negative than that for the binding between CNPs through neutral amide group and DNA backbone phosphate (− 47.3 kJ/mol) as well as the binding between CNPs through neutral group and DNA bases (most negative − 21.7 kJ/mol).

It is the phosphatase, that takes the primary responsibility of CNPs in cell swelling, bursting, and recovery, as phosphorylation and dephosphorylation of fibronectin regulates the cell attachment/detachment and perhaps meditates the relocation of water channel protein AQP5 (Yalak et al. 2019; Bork and Doolittle 1993; Bhalla et al. 1999).

CNPs can induce cell death through the regulation of osmosis-related phenotype. The very nature of the reversibility of phosphatase may, therefore, determine the respectability of observed carbopoptosis.

The mechanisms of drug resistance to PARPi can be through two pathways, BRCA1-mediated double-stranded DNA repair and dysregulation of kinase signaling and potential cancer stem cells (Lord and Ashworth 2017; Shibue and Weinberg 2017). In principle, soybean and beet, derived nanoparticles, exhibit nanozyme function that is related to natural compounds or through a "sugar" mediated nanozyme effect leading to dephosphorylation while phosphorylation are essential in modification and regulation of DNA repair proteins with their function (Benassi et al. 2021; Mu et al. 2021; He et al. 2021). Nevertheless, further studies and potential applications of food product-derived nanozyme deserve more in-depth exploration.

Carbon-based nanozyme materials have been well studied and applied to various practices regarding their antitumor and antimicrobial effects. However, so far carbon-based nanozymatic activities are limited to oxidase, peroxidase, superoxide dismutase and catalase activities (Nazarbek et al. 2021; Ouyang et al. 2021; Shen et al. 2022). The antitumor effect developed by nanozymes with oxidizing characteristics can be attributed to the reactive oxygen species (ROS) (Xie et al. 2019; He et al. 2021; Nazarbek et al. 2021). Different elements, natural products or metal-doped carbon-based nanoparticles are developed to be used as sensor, anti-cancer therapeutic agents (Yu et al. 2021; Zhu et al. 2021; Shukla et al. 2021; Kazybay et al. 2022; Xie et al. 2021). However, whether this nanozyme-induced cell death is reversible is largely unknown, not to mention their roles in drug resistance and DNA repair crosstalk. Herein, we provided the new types of cell death with interesting findings: 1. Cell adhesion is essential for the CNPs mediated cell death by carbon. 2. In vitro cell data manifested the cell death dynamics with cell cycle analysis and adhesion analysis induced by CNPs. 3. PARP is the pathway and target of the CNPs induced cell death. 4. The drug resistance against PARPi developed by low-dose CNPs is likely related to phosphatase activities in cells by crosstalk.

Conclusions

At low dose, soybean and beet-derived CNPs induce PARPi resistance at least in part, through their phosphatase nanozyme crosstalk in cancer cells, whereas, at high dose, these CNPs achieve synthetic lethality with PARPi. The findings in the present work emphasize the role of dosage of nanomaterials in antitumor therapy, wherein the low dose could induce drug resistance through competitive binding with the targeting DNA. Therefore, a cocktail styled combination of CNPs, PARP inhibitor and PPi was then proposed as a novel conceptual treatment avenue to ensure "synthetic lethality" in cancer nanotechnology therapy and preventing drug resistance concomitantly.

Abbreviations

CNPs	Carbon nanoparticles
ALP	Alkaline phosphatase
HR-AFM	High-resolution atomic-force microscopy
FT-IR	Fourier transform infrared
dsDNA	Double-strand DNA
ssDNA	Single-strand DNA
DAPI	4′,6-Diamidino-2-phenylindole

Supplementary Information

The online version contains supplementary material available at https://doi.org/10.1186/s12645-022-00144-9.

Additional file 1. Video of carbon nanoparticles derived from beet induced cell death (refer to file name Beet0.5mgml.avi).

Additional file 2. Video of carbon nanoparticles derived from soybean induced cell death (refer to file name soybean0.5mgml.avi).

Additional file 3. Video of hypotonic effect on cell death induced by carbon nanoparticles derived from soybean (refer to file name hypotonicglucose2.5soy0.25mgml.avi).

Additional file 4. Video of hypertonic effect on cell death induced by carbon nanoparticles derived from soybean (refer to file name hypertonic-glucose-10_-soy0.25mg_ml.avi).

Additional file 5: Figure. S1 Carbon Nanoparticles (indicated as CNP, or CNDs) induce a novel cell death of carbopoptosis. a. Investigation of CNPs derived from soybean and beet by AFM and distribution of size counting. b. Soybean CNP induces osmosis-related cell death in PC3 cells treated with 0.25 mg/mL for times indicated upon pretreatment with 2.5M and 10M glucose, respectively. c. CNPs induced cell death at 0.1 mg/mL which can be prevented by Matrigel and fibronectin. d. Single floating cells were collected and formed spheres upon continue culture by removing CNPs. PC3 cells were collected after treatment of overnight by vehicle or 0.3 and 0.9 mg/mL and continue culture for days indicated. e, f. Cell cycle, cell death analysis by flow cytometer, or cell analyzer. PC3 or NRK cells were treated by CNPs for 2 h and subjected to analysis. **Figure. S2** Supporting Fig 5d, e. **Figure. S3** Nanozyme activity of Beet SS carbon nanoparticles which exhibit higher phosphatase activity and enhanced anchorage-independent sphere growth with less cell death. a. Nanozyme assay with the condition at pH 7 using NBT/BCIP as substrate. NBT/BCIP, and beet/beet SS, at 0.25 mg/mL in the reaction. b. A soft agar assay.

Acknowledgements
We would like to thank the students including Adilet Dautov, Balnur Bazarbayeva, Nazgul Ibragimova, Shuwen Sunchen, Lulu Liu, Yan Zhang, Alibek Ysmaiyl, Aigerim Kabulova, Saltanat Kaldar, Diana Aliyeva, Aigerim Nugmanova, Ruslan Nassyrov, and Ayagoz Meirkhanova who contributed their support, assistance or valuable comments. We thank the Nazarbayev University Faculty-Development Competitive Research Grants Program with grant ID 16392864; 15798117 (i.e.16797152;110119FD4531), and ID: 40018227; i.e. 40018290 (11022021FD2920) with title"Improving the efficacy of PARP inhibition with Sulfur-Carbon Nanodots through DNA damage response" to PI Yingqiu Xie; and ID: 15874919 to PI Haiyan Fan (i.e.110119FD4542 and 11022021FD2928) and Co-PI, YX. YX and AA thank UAEU-AUA Fellowship grant support (2019; 12R118).

Author contributions
HF synthesized carbon dots, sulfur-doped carbon dots, conducted some experiments and wrote the paper. QS performed experiments, protein sequencing, data analysis, and wrote a part of the paper. KD performed AFM, wrote a part of methods, results and revised paper. EB performed calculations, wrote the paper. LM, AN, MK, MR performed some experiments, analyzed data, and wrote methods. AA, GL, and ZC revised paper, designed and supervised experiment. CM performed bioinformatics data analysis and wrote a part of the methods. YX developed the concept, designed experiments, performed some experiments, analyzed data, and wrote the paper. All authors read and approved the final manuscripts.

Funding
This work was supported by Nazarbayev University Faculty-Development Competitive Research Grants Program with grant ID: 16392864; i.e. 15798117 (i.e.16797152;110119FD4531), and ID: 40018227; i.e. ID: 40018290 (11022021FD2920) with title"Improving the efficacy of PARP inhibition with Sulfur-Carbon Nanodots through DNA damage response" to PI Yingqiu Xie; and ID: 15874919 to PI, Haiyan Fan (i.e.110119FD4542 and 11022021FD2928) and Co-PI, Yingqiu Xie. The project is also supported by UAEU-AUA Fellowship Award to Yingqiu Xie and Amr Amin (2019; 12R118).

Availability of data and materials
Upon reasonable request, data can be provided.

Declarations

Ethics approval and consent to participate
Not applicable.

Consent for publication
Not applicable.

Competing interests
The authors declare that they have no competing interests.

Author details
[1]Department of Chemistry, School of Sciences and Humanities, Nazarbayev University, Astana 010000, Kazakhstan. [2]Key Laboratory for Applied Technology of Sophisticated Analytical Instrument of Shandong Province, Shandong Analysis and Test Center, Qilu University of Technology (Shandong Academy of Sciences), Jinan, China. [3]Department of Electrical and Computer Engineering, School of Engineering and Digital Science, Nazarbayev University, Astana 010000, Kazakhstan. [4]Faculty of Natural Sciences, Novosibirsk State University, Novosibirsk, Russia. [5]Department of Biology, School

of Sciences and Humanities, Nazarbayev University, Astana 010000, Kazakhstan. [6]Zhejiang University-Hangzhou Global Scientific and Technological Innovation Center, Hangzhou, China. [7]Department of Biochemistry, Cancer Biology, Neuroscience and Pharmacology, Meharry Medical College, Nashville, TN 37208, USA. [8]Biology Department, UAE University, 15551 Al Ain, UAE.

Received: 1 September 2022 Accepted: 27 October 2022
Published online: 28 November 2022

References

Benassi E, Fan H, Sun Q et al (2021) Generation of particle assemblies mimicking enzymatic activity by processing of herbal food: the case of rhizoma polygonati and other natural ingredients in traditional Chinese medicine. Nanoscale Adv 3:2222–2235

Bhalla DK, Gupta SK, Reinhart PG (1999) Alteration of epithelial integrity, alkaline phosphatase activity, and fibronectin expression in lungs of rats exposed to ozone. J Toxicol Environ Health A 57:329–343

Bork P, Doolittle RF (1993) Fibronectin type III modules in the receptor phosphatase CD45 and tapeworm antigens. Protein Sci 2:1185–1187

Callister SJ, Barry RC, Adkins JN, Danielsson KG, Dahlberget M et al (2006) Normalization approaches for removing systematic biases associated with mass spectrometry and label-free proteomics. J Proteome Res 5:277–286

Chen D, Li B, Lei T, Na D, Nie M, Yang Y, Congjia X, He Z, Wang J (2021) Selective mediation of ovarian cancer SKOV3 cells death by pristine carbon quantum dots/Cu2O composite through targeting matrix metalloproteinases, angiogenic cytokines and cytoskeleton. J Nanobiotechnology 19:68. https://doi.org/10.1186/s12951-021-00813-8

Clarke N, Wiechno P, Alekseev B, Sala N, Jones R, Kocak I et al (2018) Olaparib combined with abiraterone in patients with metastatic castration-resistant prostate cancer: a randomised, double-blind, placebo-controlled, phase 2 trial. Lancet Oncol 19:975–986

Coleman RL, Sill MW, Bell-McGuinn K, Aghajanian C, Gray HJ, Tewari KS et al (2015) A phase II evaluation of the potent, highly selective PARP inhibitor veliparib in the treatment of persistent or recurrent epithelial ovarian, fallopian tube, or primary peritoneal cancer in patients who carry a germline BRCA1 or BRCA2 mutation—an NRG Oncology/Gynecologic Oncology Group study. Gynecol Oncol 137:386–391

Cox J, Mann M (2008) MaxQuant enables high peptide identification rates, individualized ppb-range mass accuracies and proteome-wide protein quantification. Nat Biotechnol 26:1367–1372

da Huang W, Sherman BT, Lempicki RA (2009) Systematic and integrative analysis of large gene lists using DAVID bioinformatics resources. Nat Protoc 4:44–57

D'Arcy MS (2019) Cell death: a review of the major forms of apoptosis, necrosis and autophagy. Cell Biol Int 43:582–592

Doncheva NT, Morris J, Gorodkin J, Jensen LJ (2019) Cytoscape stringApp: network analysis and visualization of proteomics data. J Proteome Res 18:623–632

Fabregat A, Sidiropoulos K, Viteri G, Forner O, Marin-Garcia P, Arnau V, D'Eustachio P, Stein L, Hermjakob H (2017) Reactome pathway analysis: a high-performance in-memory approach. BMC Bioinformatics 18:142

Fang Y, Tian S, Pan Y, Li W, Wang Q, Tang Y et al (2020) Pyroptosis: A new frontier in cancer. Biomed Pharmacother 121:109595

Fujioka M, Wu C, Kubo N, Zhao G, Inoishi A, Okada S, Demura S, Sakata H, Ishimaru M, Kaiju H, Nishii J (2017) J Am Chem Soc 139:17987–17993

Gong N, Ma X, Ye X, Zhou Q, Chen X, Tan X et al (2019) Carbon-dot-supported atomically dispersed gold as a mitochondrial oxidative stress amplifier for cancer treatment. Nat Nanotechnol 14:379–387

He D et al (2021) Recent progress in carbon-dots-based nanozymes for chemosensing and biomedical applications. Chinese Chemical Letters ISSN. https://doi.org/10.1016/j.cclet.2021.03.078

Hsu PC, Chen PC, Ou CM, Chang HY, Chang HT (2013) Extremely high inhibition activity of photoluminescent carbon nanodots toward cancer cells. J Mater Chem B 1:1774–1781

Kad NM, Wang H, Kennedy GG, Warshaw DM, Van Houten B (2010) Collaborative dynamic DNA scanning by nucleotide excision repair proteins investigated by single- molecule imaging of quantum-dot-labeled proteins. Mol Cell 37:702–713

Kanehisa M, Sato Y, Furumichi M, Morishima K, Tanabe M (2019) New approach for understanding genome variations in KEGG. Nucleic Acids Res 47:D590–D595

Kazybay B et al (2022) Network pharmacology with experimental investigation of the mechanisms of rhizoma polygonati against prostate cancer with additional herbzymatic activity. ACS Omega 7:14465–14477. https://doi.org/10.1021/acsomega.1c03018

Kim Y, Kim A, Sharip A, Sharip A, Jiang J, Yang Q et al (2017) Reverse the resistance to PARP inhibitors. Int J Biol Sci 13:198–208

Kirwale S, Pooladanda V, Thatikonda S, Murugappan S, Khurana A, Godugu C (2019) Selenium nanoparticles induce autophagy mediated cell death in human keratinocytes. Nanomedicine (lond) 14:1991–2010

Kokorina AA, Bakal AA, Shpuntova DV, Kostritskiy AY, Beloglazova NV, De Saeger S, Sukhorukov GB, Sapelkin AV, Goryacheva IY (2019) Gel electrophoresis separation and origins of light emission in fluorophores prepared from citric acid and ethylenediamine. Sci Rep 9(1):14665. https://doi.org/10.1038/s41598-019-50922-6

LeCory GE, Messina F, Sciortino A, Bunker CE, Wang P, Fernando KAS, Sun Y-P (2017) Characteristic excitation wavelength dependence of fluorescence emissions in carbon "Quantum" Dots. J Phys Chem C 121:28180–28186

Li CL, Ou CM, Huang CC, Wu WC, Chen YP, Lin TE (2014) Carbon dots prepared from ginger exhibiting efficient inhibition of human hepatocellular carcinoma cells. J Mater Chem B 2:4564–4571

Li M-Y et al (2018) Role of surface charge on the interaction between carbon nanodots and human serum albumin. Spectrochim Acta Part A Mol Biomol Spectrosc 204:484–494. https://doi.org/10.1016/j.saa.2018.06.082

Chunquan Li lab KnockTF online database http://www.licpathway.net/KnockTF/analysis/analysis_submit_gene.php Accessed Apr 2002

Lord CJ, Ashworth A (2017) PARP inhibitors: synthetic lethality in the clinic. Science 355:1152–1158. https://doi.org/10.1126/science.aam7344
Lou Q, Ni Q, Niu C, Wei J, Zhang Z, Shen W, Shen C, Qin C, Zheng G, Liu K, Zang J, Dong L, Shan CX (2022) Carbon nanodots with nearly unity fluorescent efficiency realized via localized excitons. Adv Sci (weinh). https://doi.org/10.1002/advs.202203622
Ma X, Sun J, Zhong L, Wang Y, Huang Q, Liu X et al (2019) Evaluation of turning-sized gold nanoparticles on cellular adhesion by golgi disruption in vitro and in vivo. Nano Lett 19:8476–8487
Miao P, Han K, Tang Y, Wang B, Lin T, Cheng W (2015) Recent advances in carbon nanodots: synthesis, properties and biomedical applications. Nanoscale 7:1586–1595
Mu C, Sheng Y, Wang Q et al (2021) Potential compound from herbal food of Rhizoma Polygonati for treatment of COVID-19 analyzed by network pharmacology: viral and cancer signaling mechanisms. J Funct Foods 77:104149
Nazarbek G, Kutzhanova A, Nurtay L, Mu C, Kazybay B et al (2021) Nano-evolution and protein-based enzymatic evolution predicts the novel types of natural product nanozyme of traditional Chinese medicine: cases of herbzymes of Taishan-Huangjing (Rhi-zoma polygonati) and Goji (Lycium chinense). Nanoscale Adv 3:6728–6738
Nurkesh AA, Sun Q, Fan H, Dukenbayev K, Tsoy A, Altaikyzy A et al (2019) Date pit carbon dots induce acidic inhibition of peroxidase and disrupt DNA repair in antibacteria resistance. Glob Chall 3:1900042
Oliveros JC (2007–2015) Venny. An interactive tool for comparing lists with Venn's diagrams. https://bioinfogp.cnb.csic.es/tools/venny/index.html
O'Neil NJ, Bailey ML, Hieter P (2017) Synthetic lethality and cancer. Nat Rev Genet 18:613–623. https://doi.org/10.1038/nrg.2017.47
Ouyang Y, Biniuri Y, Fadeev M, Zhang P, Carmieli R, Vázquez-González M, Willner I (2021) Aptamer-modified Cu^{2+}-functionalized C-Dots: versatile means to improve nanozyme activities-"Aptananozymes." J Am Chem Soc 143:11510–11519. https://doi.org/10.1021/jacs.1c03939
Sai L et al (2017) Protein-derived carbon nanodots with an ethylenediamine-modulated structure as sensitive fluorescent probes for Cu2+ detection. RSC Adv 7:16608–16615
Sandberg A, Lindell G, Källström BN et al (2012) Tumor proteomics by multivariate analysis on individual pathway data for characterization of vulvar cancer phenotypes. Mol Cell Proteomics 11(M112):016998
Shannon P, Markiel A, Ozier O, Baliga NS, Wang JT, Ramage D et al (2003) Cytoscape: a software environment for integrated models of biomolecular interaction networks. Genome Res 13:2498–2504
Shen C et al (2022) Near-Infrared chemiluminescent carbon nanogels for oncology imaging and therapy. SmartMat 3:269–285
Shi YB (1995) Cell-cell and cell-ECM interactions in epithelial apoptosis and cell renewal during frog intestinal development. Cell Biochem Biophys 27:179–202. https://doi.org/10.1007/BF02738109
Shibue T, Weinberg RA (2017) EMT, CSCs, and drug resistance: the mechanistic link and clinical implications. Nat Rev Clin Oncol 14:611–629
Shukla AK, Sharma C, Acharya A (2021) Bioinspired metal-free fluorescent carbon nanozyme with dual catalytic activity to confront cellular oxidative damage. ACS Appl Mater Interfaces 13:15040–15052
Singh S, Singh MK, Das P (2018) Visual detection of cyclobutane pyrimidine dimer DNA damage lesions by Hg(2+) and carbon dots. Anal Chim Acta 1016:49–58
Szklarczyk D, Gable AL, Lyon D, Junge A, Wyder S, Huerta-Cepas J, Simonovic M, Doncheva NT, Morris JH, Bork P, Jensen LJ, von Mering C (2019) STRING v11: protein-protein association networks with increased coverage, supporting functional discovery in genome-wide experimental datasets. Nucleic Acids Res 47:D607-613
Vivo M, Fontana R, Ranieri M, Capasso G, Angrisano T, Pollice A et al (2017) p14ARF interacts with the focal adhesion kinase and protects cells from anoikis. Oncogene 36:4913–4928
Wang H, Su W, Tan M (2020) Endogenous fluorescence carbon dots derived from food items. Innovation 1:100009
Wiśniewski JR, Zougman A, Nagaraj N, Mann M (2009) Universal sample preparation method for proteome analysis. Nat Methods 6:359–362
Xiao H, Chen Y, Alnaggar M (2019) Silver nanoparticles induce cell death of colon cancer cells through impairing cytoskeleton and membrane nanostructure. Micron 126:102750
Xie Y, Sun Q, Nurkesh AA, Lu J, Kauanova S, Feng J (2017) Dysregulation of YAP by ARF stimulated with tea-derived carbon Nanodots. Sci Rep 7:16577
Xie Y, Fan H, Lu W, Yang Q, Nurkesh A, Yeleussizov T et al (2019) Nuclear MET requires ARF and is inhibited by carbon nanodots through binding to phospho-tyrosine in prostate cancer. Oncogene 38:2967–2983
Xie Y et al (2021) Network pharmacology and experimental investigation of Rhizoma polygonati extract targeted kinase with herbzyme activity for potent drug delivery. Drug Deliv 28:2187–2197. https://doi.org/10.1080/10717544.2021.1977422
Xu Q, Pu P, Zhao J, Dong C, Gao C, Chen Y, Chen J, Liu Y, Zhou H (2015) Preparation of highly photoluminescent sulfur-doped carbon dots for Fe(iii) detection. J Mater Chem A3:542–546
Yalak G, Shiu JY, Schoen I, Mitsi M, Vogel V (2019) Phosphorylated fibronectin enhances cell attachment and upregulates mechanical cell functions. PLoS ONE 14:e0218893
Yu B et al (2021) Defect engineering enables synergistic action of enzyme-mimicking active centers for high-efficiency tumor therapy. J Am Chem Soc 143:8855–8865
Zhang CY, Dong X, Gao J, Lin W, Liu Z, Wang Z (2019) Nanoparticle-induced neutrophil apoptosis increases survival in sepsis and alleviates neurological damage in stroke. Sci Adv. https://doi.org/10.1126/sciadv.aax7964
Zheng GS, Shen CL, Lou Q, Han JF, Ding ZZ, Deng Y, Wu MY, Liu KK, Zang JH, Dong L, Shan CX (2022) Meter-scale chemiluminescent carbon nanodot films for temperature imaging. Mater Horiz 9:2533–2541. https://doi.org/10.1039/d2mh00495j
Zhu Y et al (2021) A facile strategy for synthesis of porous Cu2O nanospheres and application as nanozymes in colorimetric biosensing. J Mater Chem B 9:3533–3543

Publisher's Note